A thermochemical understanding of the factors that govern the growth of chemical bath deposition of Cu2O thin films

T. Hildebrandt, L. Mathon-Claudon, Negar Naghavi

A thermochemical understanding of the factors that govern the growth of chemical bath deposition of Cu_2O thin films

T. Hildebrandt[a], *L. Mathon-Claudon*[b], *N. Naghavi*[b*]

[a]EDF R&D, 18 boulevard Thomas Gobert, 91120 Palaiseau, France

[b]Institut Photovoltaïque d'Île-de-France (IPVF), CNRS, UMR 9006, 91120 Palaiseau, France,

Email :negar.naghavi@chimieparistech.psl.eu, Tel : +33 1 69865971

Abstract

A simple room-temperature chemical bath deposition technique, inspired by the Felhling method, was used to deposit nanocrystalline cuprous oxide (Cu_2O) thin films. The process involved a mixture of copper sulfate, sodium potassium tartrate, and sodium hydroxide. A thermochemical analysis explored how pH and complexing agent concentration affected $Cu(OH)_2$ solubility and subsequent Cu_2O growth using species repartition diagrams. The study is conducted by fixing the [tartrate]/[Cu] ratio at 10, while varying pH, deposition time, and temperatures from room temperature to 80 °C. While oxide nucleation and growth began at pH=9, denser and more uniform films formed at pH=10 and 11, corresponding to the co-existing domain of copper hydroxo and copper tartrate complexes. Notably, regardless of pH, temperature, or reducing agent, the Cu_2O (111) facets appear to be selectively stabilized. The introduction of an aldehyde reducing agent such as glucose had little effect on the growth of Cu_2O layers at room temperature but promoted the formation of Cu^0 at 80°C.

1. Introduction

Cu_2O is an abundant and non-toxic native p-type semiconductor, characterized by a direct band gap of 2.1 eV[1] and a high absorption coefficient spanning the violet to green solar spectrum [2, 3]. In addition, it has relatively high charge carrier mobility among p-type oxides, is easy to deposit as a thin film, and its morphology and nanoparticle size can be easily controlled. [4, 5]. All these properties make Cu_2O suitable not only as an absorber

converting solar energy into electrical or chemical energy and fuels but also as a catalyst. As a result, Cu_2O has been used in a wide range of applications, including solar cells[6-8], light emitting diodes, optoelectronic components, optical, gas, and bio sensors[9], photocatalysts for CO_2 reduction[10-13] and water splitting under visible light irradiation[14-17].

Over the past decade, thin film deposition of Cu_2O has been the subject of intense research because of its applications in the various fields mentioned above. Various deposition methods[18], including sputtering[19], electrodeposition[16, 20-22], chemical vapor deposition, and chemical bath deposition (CBD) [23, 24], have been used. While most of these techniques remain costly to implement due to their reliance on advanced equipment., the Chemical Bath Deposition Method (CBD) is appealing because it does not require expensive vacuum systems or other specialized apparatus. CBD, has been widely used for the formation of chalcogenide [25, 26] or oxide thin films[25, 27, 28]. It is a well-known technique for depositing thin films through the use of a controlled chemical reaction [29] [30].

In chemical bath deposition, substrates are immersed in deposition solutions that contain metal salt, a pH regulator, and a complexing agent. The pH level, the nature of the complexing agent, the deposition temperature, and the substrate's nature collectively impact the growth rates, characteristics, and structure of the resulting thin films[29]. For the deposition of Cu_2O using chemical bath deposition, $CuSO_4$ is commonly used as a metal salt, and NaOH as a pH regulator. Various complexing agents, such as ethylenediaminetetraacetic acid[31], tartrate[32], citrate[24], ammonia[33], hexadecyl trimethyl ammonium bromide[34], sodium L-ascorbate[30], and formaldehyde, have been used in the literature. In chemical deposition synthesis, the complexing agent forms stable complexes with metal ions within the solution, which hinders the precipitation of $Cu(OH)_2$. This, in turn, leads to a slower nucleation rate and a more controlled growth of the Cu_2O layers. In alkaline solutions, these complexes coexist with copper hydroxide complexes; nevertheless, there have been no substantial analytical studies conducted to gain a deeper understanding of how these various complexes influence the growth and structure of the deposited layers. In this study, we introduce a simple approach to prepare Cu_2O thin films using very low concentrations of copper precursors (0.01 M) and complexing agents (0.1

M). This method takes inspiration from Fehling's technique. The Fehling approach is commonly used in aldehyde analysis. This method is based on the reduction, by glucose, of Fehling's liquor, a mixture of copper sulfate and sodium potassium tartrate in the presence of sodium hydroxide. When an aldehyde, such as glucose, is added to the Fehling reagent at a basic pH, the complex's Cu^{2+} ions are converted to Cu^{+} ions, resulting in a red copper(I) oxide precipitate ($Cu_2O(s)$).

Based on this approach, our study uses sodium potassium tartrate ($NaKC_4H_4O_6$) as a complexing agent, which is combined with a basic aqueous copper (II) sulfate solution. The study is based initially on the development of a thermodynamic model to better understand the chemistry of the Cu_2O synthesis process at room temperature. This model is based on the interaction between pH and the relative concentration of the complexing agent to the copper precursor ([tartrate]/[Cu]), examining their effects on the composition of the complexing compounds in solution, the solubility of $Cu(OH)_2$, and the subsequent growth of Cu_2O via species distribution diagrams.

Once the method has been developed, the influence of pH, deposition time, temperature, and the incorporation of a reducing agent such as glucose into the solution on the properties of the thin films is studied and compared with the results of thermodynamic calculations.

2. Methods

The thin films were deposited on a 2,5x2,5 cm^2 glass substrates (2 mm thick) covered by 300 nm molybdenum (Mo) thin films. Glass/Mo substrate is used as it could be a good substrate both as a metal electrode for future catalytic analysis and as a back contact for the preparation of thin film solar cells. No treatment of the substrate is done before deposition. Mo thin films were deposited by radio frequency (RF) (13.56 MHz) sputtering using Mo target (purity, 99.95%). The pressure was varied by adjusting the argon flow (purity, 99.9997%) while keeping the RF power at 600 W. The sputtered Mo layer has a cubic crystal structure with a preferential growth orientation in [110].

All reagents are of analytical grade and used without further purification. The preparation processes for Cu_2O thin films are shown in Table 1.

Metallic salt	Complexing agent	Reducing agent	pH
$CuSO_4$ (ThermoFisher scientific, 99,999 %)	Sodium and potassium Tartrate (VWR, 99.0-102.0%)	Glucose anhydrous, (fisher scientific, 99 %)	pH (adjusted by varying the NaOH concentration)
0.01 M	from 0.01 to 0.5 M	from 0.01 to 0.5 M	from 7 to 12

Table 1. Deposition Parameters for Cu_2O Synthesis

Deposition of Cu_2O is carried out from a 0.01M of aqueous solution of $CuSO_4$ with the addition of sodium potassium tartrate $NaKC_4H_4O_6$ and glucose at basic pH. For the deposition, the pH of the solution was varied between 8 and 12 using NaOH. The temperature was adjusted at 25, 50, and 80°C and the deposition time was varied between 30s and 1 hour.

Thin-film structural properties were determined by X-ray diffraction under Bragg Brentano conditions (XRD) for crystallinity determination and phase detection with a PANalytical Empyrean equipment using Cu-Kα radiations. (1.5419Å). The surface morphology of the samples was investigated by scanning electron microscopy (SEM) using a Leo Supra 35 field emission gun (FEG) with 15 kV voltage. The thickness of the layers have been measured using Dektak Burker profilomete

3. Results

3.1. Copper species repartition–pH diagrams

The existence domain of Cu_2O corresponds to the stability domain of the Cu^+ ion in solution in the Pourbaix diagram. As a result, the pH of the solution plays an important role in the formation of a pure Cu_2O layer. In a basic medium, Cu^{2+} copper ions precipitate in the form of the poorly soluble hydroxide $Cu(OH)_2$ [35]. A complexing agent, such as sodium or potassium tartrate, can form stable complexes with metal ions in the solution

and prevent the precipitation of $Cu(OH)_2$ hydroxide. The latter increases $Cu(OH)_2$ solubility and thus stabilizes copper (II) via complexation rather than precipitation.

An important point is to understand the deposition solution chemistry and especially the copper species involved in the deposition process. This can be done by the study of the species distribution diagram which can provide a better understanding of the reactions that are likely to occur in solution, even if this information does not take the kinetics of the reactions into account. The distribution diagram took into account the pH, total concentrations of copper ions dissolved in the solution, and all soluble complexes with tartrate acid and hydroxide that could form in the system. In an aqueous solution, Cu(II) soluble species are Cu^{2+} and hydroxide or tartrate complexes. The concentration of the latter is related to Cu^{2+} concentration by the equilibrium reaction:

$$Cu^{2+} + iL \Leftrightarrow CuLi^{2+}$$

$$\beta_i^L = \frac{[CuL_i^{2+}}{[Cu^{2+}][L]^i}$$

where L represents a ligand, OH^- or T^{2-} in the present work, $\beta^L{}_i$ the stability constant of the complex $CuL_i{}^{2+}$ and *i is* the coordination number.

From the values of $\beta^L{}_i$, it is possible to calculate the ratio between a soluble copper species and the total copper concentration in solution as a function of pH. $Cu(OH)_2$ solid phase is also taken into account. This work has been performed for different portions of [Tartrate]/[Cu] and the results are presented as species repartition–pH diagrams in Figure 1.

The overall reaction of Cu_2O formation after the complexation of copper by tartrate anion (T^{2-}) can be written as:

$$2[CuT_2]^{2-} + 2OH^- + 2e^- \rightarrow Cu_2O + H_2O + 4T^{2-} \quad \text{Eq.1}$$

based on the two following sub-reactions :

$$2[CuT_2]^{2-} + 4OH^- \rightarrow 2Cu(OH)_2(s) + 4\,T^{2-} \quad \text{Eq.2}$$

$$2Cu(OH)_2(s) + 2H^+ + 2e^- \rightarrow Cu_2O(s) + 3H_2O \quad \text{Eq.3}$$

In fact, for a metal cation M^{m+} complexed by i ligands L^{k-}, the steps to forming the oxide $MO_{n/2}$ can be formulated as the following reactions:

dissociation of water: $nH_2O \rightarrow n\,OH^- + nH^+$ Eq.4

displacement of Ligands : $nOH^- + M(L)_i^{(n-ik)+} \rightarrow M(OH)_n(s) + iL^{k-}$ Eq.5

deprotonation to form oxide : $M(OH)_n(s) \rightarrow MO_{n/2}(s) + n/2\ H_2O$ Eq.6

Total reaction : $M(L)_i^{(n-ik)} + n/2\ H_2O \rightarrow MO_{n/2}(s) + nH^+ + iL^{k-}$ Eq.7

The reactions that must be considered are complex formation reactions. These reactions are described as equilibrium reactions. The concentration of soluble species is related to the concentration of free metal ions (M^{m+}) based on the equilibrium reactions (8) and (9):

$$M^{m+} + nL^{l} \leftrightarrows M(L)_n^{m-nl} \qquad \textbf{Eq. 8}$$

$$\beta_n^L = \frac{[M(L)_n^{m-nL}]}{[M^{m+}][L^l]^n} \qquad \textbf{Eq. 9}$$

Where L^l represents a ligand, β_n^L is the stability constant of the complex and n is the coordination number of Ligand[26, 36, 37].

In the aqueous phase, copper (II) ions can form complex compounds with a variety of organic and inorganic ligands. In this study, $CuSO_4$ -Tartare (T) solution with NaOH as a pH-correcting agent is used for the chemical bath deposition of Cu_2O.

Copper hydroxo-complexes $[Cu(OH)_n]^{2-n}$ and tartrate complexes $[Cu(T)n]^{2-n}$ can exist and/or coexist in this system.

We reported in **Table 2**. the values of all soluble hydroxide, tartrate, and sulfates complexes at a temperature of 25 °C calculated from the corresponding Gibbs free energy values [38]. The hydroxide complexes considered are:$[Cu(OH)]^+$, $[Cu(OH)_2]$, $[Cu(OH)_3]^-$ and $[Cu(OH)_4]^{2-}$

and the Cu-tartrate complexes are: CuT, $[Cu(T)_2]^{2-}$, $[Cu(T)_3]^{4-}$, $[Cu(T)_4]^{6-}$

whose stability constants are listed in **Table 2**.

Only one solid species is considered: $Cu(OH)_2$ the pK_S of which is also reported in Table **1Table 2**. The ionic strength is not taken into account here. The acidity constants of H_2T, HT^-, H_2SO_4, and HSO_4^- species have been also calculated and are reported in **Table 2**.

The ratio between a soluble copper species and the total copper concentration in the solution can be calculated using the values of β_n^L.

Table 2. Stability constants of complexes, solubility products, and acidity constants at room temperature for the system Cu-T-H_2O

Dissolved species	**Log β**	**Solid species**	**pKs**	**Acid speicies**	**PKA**
$\mathbf{CuOH^+}$	6.5	$Cu(OH)_2$	18,90	H_2T	3.22
$\mathbf{Cu(OH)_2}$	16.2			HT^-	4.85
$\mathbf{[Cu(OH)_3]^-}$	26.6			H_2SO_4	-1.91
$\mathbf{[Cu(OH)_4]^{2-}}$	39.7			HSO_4^-	1.98
$\mathbf{CuT}$	3.2				
$\mathbf{[CuT_2]^{2-}}$	5.1				
$\mathbf{[CuT_3]^{4-}}$	4.8				
$\mathbf{[CuT_4]^{6-}}$	6.5				

Based on these values and a details thermodynamic calculation (See Appendix for other values), Figure 1 shows the effect of [tartrate]/[Cu] ratios ranging from 0 to 25 on the distribution of copper soluble species for 0.01M $CuSO_4$ and tartrate concentrations of 0 M (a), 0.01M (b), 0.1 M (c), and 0.25M (d). For that, we took into account the initial concentrations of $CuSO_4$, and tartrate that are known.

As observed (Figure 1), in the as-prepared alkaline solution the Cu(II) ions tend to form complex compounds with tartare, and two types of complexes can exist: copper hydroxo-complexes $[Cu(OH)_n]^{2-n}$ and copper tartrate-complexes $[Cu(T)_n]^{2-n}$. The dependence of the $[Cu(T)_2]$ concentration on the pH value of the reaction mixture indicates that at lower pH the solution mainly contains $[Cu(T)_n]^{2-n}$, whereas at higher pH $[Cu(OH)_n]^{2-n}$ dominates.

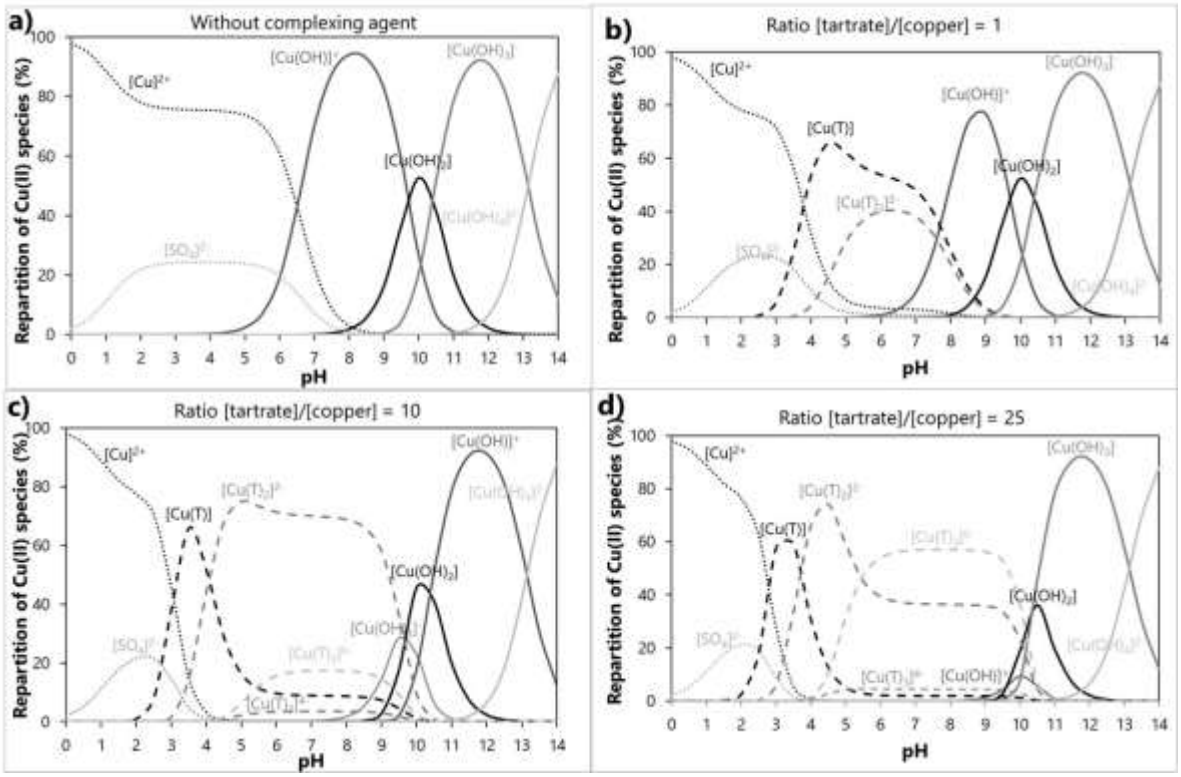

Figure 1. Repartition of the copper species as a function of pH for 0.01 M, $CuSO_4$, and tartrate concentrations of a) 0 M b) 0.01M, [tartrate]/[Cu]=1, and c) 0.1 M, [tartrate]/[Cu]=5 and d) 0.25 M, [tartrate]/[Cu]=10 at room temperature

In the absence of tartrate (as shown in Figure 1a), the concentration of free copper ions drops dramatically below pH 6, and copper-hydroxide complexes take over. When tartrate is added, all copper(II) in solution is present as complex compounds rather than free Cu^{2+} cations for pH greater than 3. Furthermore, increasing the tartrate concentration from 0.01 to 0.25 M raises the pH of the existing domain of copper-hydroxide complexes from 6 to 11. When the tartrate concentration rises from 0.01 to 0.25 M (Figure 1 b) c) and d)), the pH values in the solution containing free copper ions fall from pH=6 to pH=3.

The increase of tartrate amount also impacts directly on the concentration of [CuT], $[Cu(T)_2]^{2-}$, $[Cu(T)_3]^{4-}$ and $[Cu(T)_4]^{6-}$ complexes as a function of pH. The proportion of copper tartrate complexes as a function of tartrate concentration is shown in Figure 2 for pH values of 7, 9, 10, and 12.

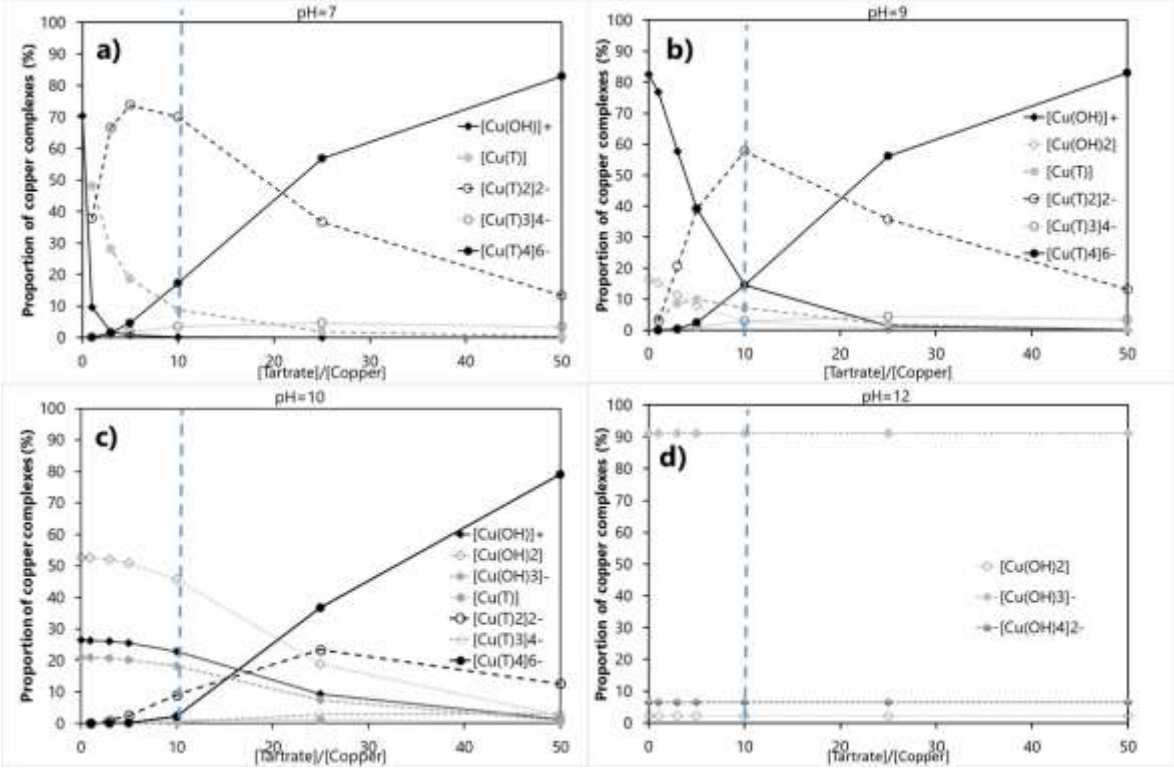

Figure 2. The proportion of copper species as a function of tartrate concentration for pH of a) 7, b) 9, c) 10, and d) 12.

It is interesting to note that for pH=9 and 10 both copper hydroxo-complexes and copper tartrate-complexes co-exist in the solution for [tartrate]/[Cu] between 10 and 20 with a predominance of copper tartrate-complexes for pH=9 and copper hydroxo-complexes for pH=10. For lower and higher pH (7 and 12) only copper tartrate-complexes or copper hydroxo-complexes exist respectively in the solution whatever [tartrate]/[Cu] fraction. It should be noted that as the pH rises above 10, more tartrate is needed to complex the copper and prevent the formation of copper-hydroxy-complexes. For pH 7 to 10 and [tartrate]/[Cu] concentrations less than 25, the predominant copper-tartrate complexes are $[Cu(T)_2]^{2-}$ and $[Cu(T)_4]^{6-}$. However, after pH=10, copper-hydroxy-complexes take over. It is expected that as the concentration of the complexing agent increases, complexes with a high coordination number will become the dominant species in solution [39]. This holds for pH levels up to 10 and tartrate concentrations higher than 20. To avoid $Cu(OH)_2$ precipitation at pH>10, we need more than 25 equivalents of [tartrate]/[Cu].

Based on this theoretical study, we investigated in the following section the effect of pH and [tartrate]/[Cu] on the nucleation, structure, and morphology of the Cu_2O layers.

3.2. Impact of the pH on the formation of Cu_2O for deposition baths with and without glucose

CBD deposition must take place in conditions that favor heterogeneous growth on the substrate over homogeneous precipitation in the solution, which can be achieved by precisely controlling the degree of supersaturation [27]. As the complexing agent aids in lowering the concentration of free metal ions and slowing hydrolysis reactions to prevent rapid bulk precipitation of the desired product, the first step is to select an appropriate [tartrate]/[Cu] ratio. Based on thermodynamic studies and a quick screening of the variation of [tartrate]/[Cu] for a $CuSO_4$ concentration of 0.01 M, it was observed that when the ratio of [tartrate]/[Cu] is less than 1, there is quasi-instantaneous precipitation of $Cu(OH)_2$, as predicted by thermodynamic diagrams. The best [tartrate]/[Cu] ratio is between 2 and 15. Based on this screening, the [tartrate]/[Cu] ratio was set to 10 for the following studies. Thus the reagent concentrations were set at [$CuSO_4$] = 0.01M and [tartrate] = 0.1 M. The pH of the solution was adjusted by varying the NaOH concentration ranging from 8 to 12 in steps of 0.5. The reactions took place at 25°C for 15 min.

The impact of a reducing agent such as glucose on the growth of these thin films has been also investigated. For that, the results are compared to the same bath with the addition of [glucose] = 0.1 M.

Figure 3 and Figure 4 show a comparison of the morphology and X-ray diffraction patterns of deposited films with and without glucose additions at pH levels ranging from 8 to 12.

SEM images (Figure 3) show that the deposition density and grain sizes increased from pH=9 to pH=11.5. At pH 9 very dispersed nuclei form grains are observed with or without glucose. The deposition becomes dense and homogeneous at pH values of 10 and 11. When the pH exceeds 11, the grains are well-defined but less covered, and the crystal size increases. When no glucose is used, the grains take on a more precise cubic shape. The sharpness of the grains seems to be reduced when glucose is added during the deposition process while a similar trend in size and substrate covering is observed. These results clearly show that dense and homogenous films are mainly obtained for pH=10 and 11 which, based on specification diagrams, corresponds to the co-existing domain of both

copper hydroxo and copper tartrate complexes in the solution. Increasing the alkalinity during preparation, leading to the presence of mainly Cu-hydroxo-complexes in the solution, reduce the density of the layers and an increase in particle size with little variation in morphology. The addition of glucose seems to have mainly primary effects on the visual morphology of Cu_2O with higher grain size for pH between 10 and 11 and less cubic-like morphologies at higher pH.

To assess the structural evolution of thin films, XRD analyses are also performed. The XRD structural analysis of depositions (Figure 4) clearly shows the formation of pure Cu_2O from pH=10 for solutions without glucose and from pH=9 for solutions with glucose. Peaks in the XRD patterns are indexed as the (110), (111), (200), (220), (311), and (222) reflections, with a preferential orientation along the (111) axis. The high intensity of the (111) diffraction peak could indicate the octahedral structure of Cu_2O where more 111 surfaces are formed. There is no evidence of Cu, CuO, or $Cu(OH)_2$, indicating that thin films containing pure Cu_2O phase can be obtained for solutions with pH greater than 9, regardless of the presence or absence of glucose. Nonetheless, a doubling of the peaks is visible at higher pH for films containing glucose. For all deposits, the relative intensity of the peaks is nearly identical. When the (111) and (200) diffraction peaks become more similar in intensity, 100 truncated octahedral Cu_2O particles can be obtained [40]. Previous works [41] demonstrated that $[Cu(OH)_n]^{2-n}$ promotes the growth of Cu_2O crystals along the (111) axis and $[Cu(T)_n]^{2-n}$ promotes the growth of Cu_2O crystals along the (100) axis. This is not the case with our films, where a higher concentration of $[Cu(OH)_n]^{2-n}$ or $[Cu(T)_n]^{2-n}$, both leads to stabilization of Cu_2O (111) facets whatever the addition or not of glucose.

It has also been reported that when the (111) plane grows relatively quickly in Cu_2O mono crystal, the shape of the Cu_2O crystal tends to be a cube, which could explain our samples' cubic shape. When (100) plane grows quickly, it usually takes the shape of an octahedron.

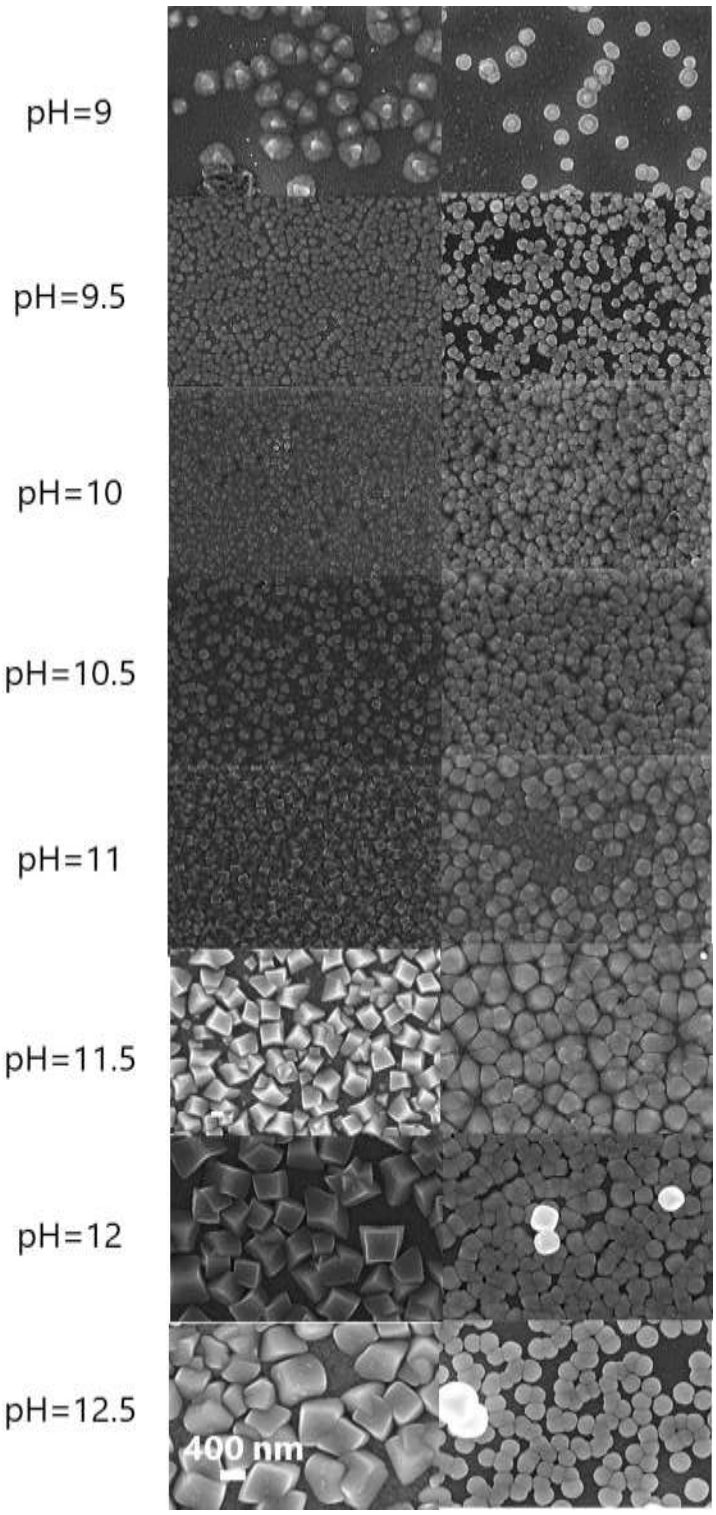

Figure 3: SEM images of Cu_2O layers deposited at pH between 9 and 12 without (left) and with (right) addition of glucose in the deposition bath

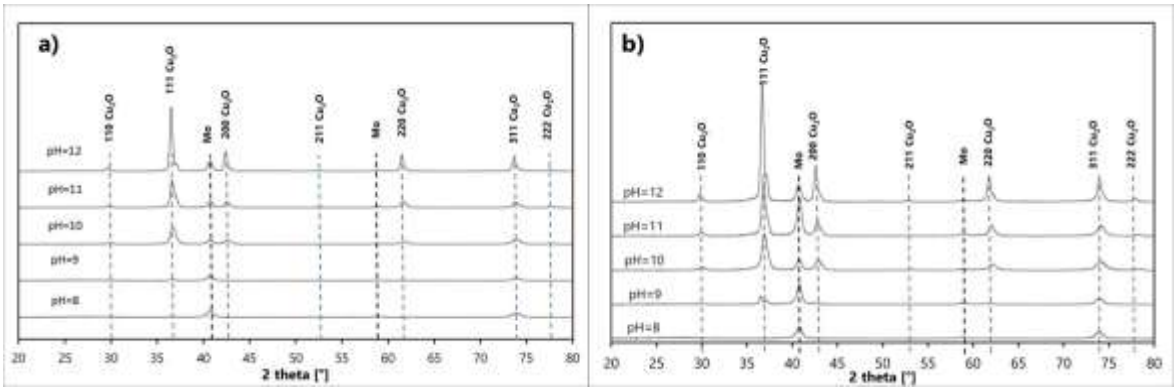

Figure 4. X-ray diffraction patterns of the Cu_2O layer deposited a) without and b) with glucose in the deposition bath at pH between 9 and 12

3.3. Reaction Time Effects:

To get a complete picture of the formation process, we studied the impact of the deposition time during the first 5 minutes on the growth of the Cu_2O layer at room temperature with and without glucose. The time-dependent study was conducted between 30 seconds and 5 minutes of deposition at room temperature. The reagent concentrations were set to [$CuSO_4$] = 0.01M, [tartrate] = 0.1 M, [glucose] = 0.1 M, and pH=10.

Figure 5 depicts the evolution of Cu_2O growth as the reaction time is varied. Regardless of whether the deposition bath contains or does not contain glucose, a seed layer forms on the substrate during the first five minutes of deposition, ensuring heterogeneous nucleation and growth during CBD of Cu_2O.

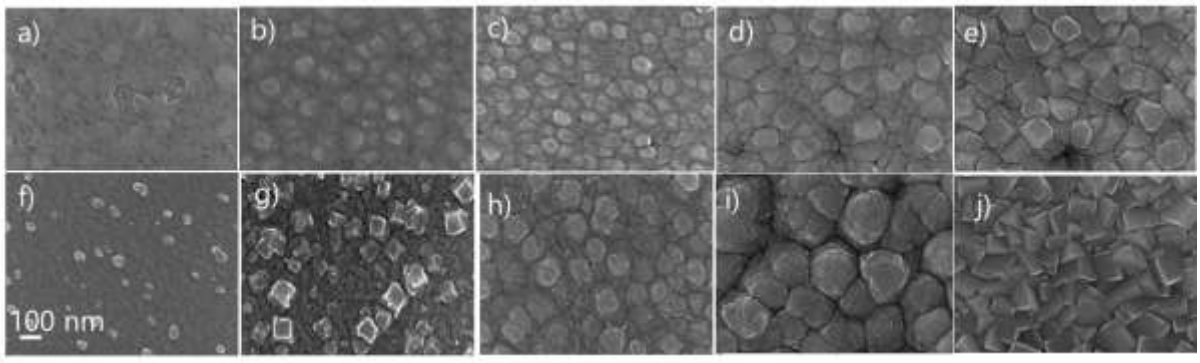

Figure 5. SEM images of Cu_2O layers deposited at pH 10 without (a-e) and with (f-j) addition of glucose at deposition times of (a,f) 30s, (b,g) 2min, (c,h) 4min, (d,i) 15 min and (e,j) 30 min

After 5 minutes of deposition, the XRD analysis reveals that this seed layer has a cubic structure crystallizing in the space group $Pn\bar{3}m$ with or without glucose (Figure 6).

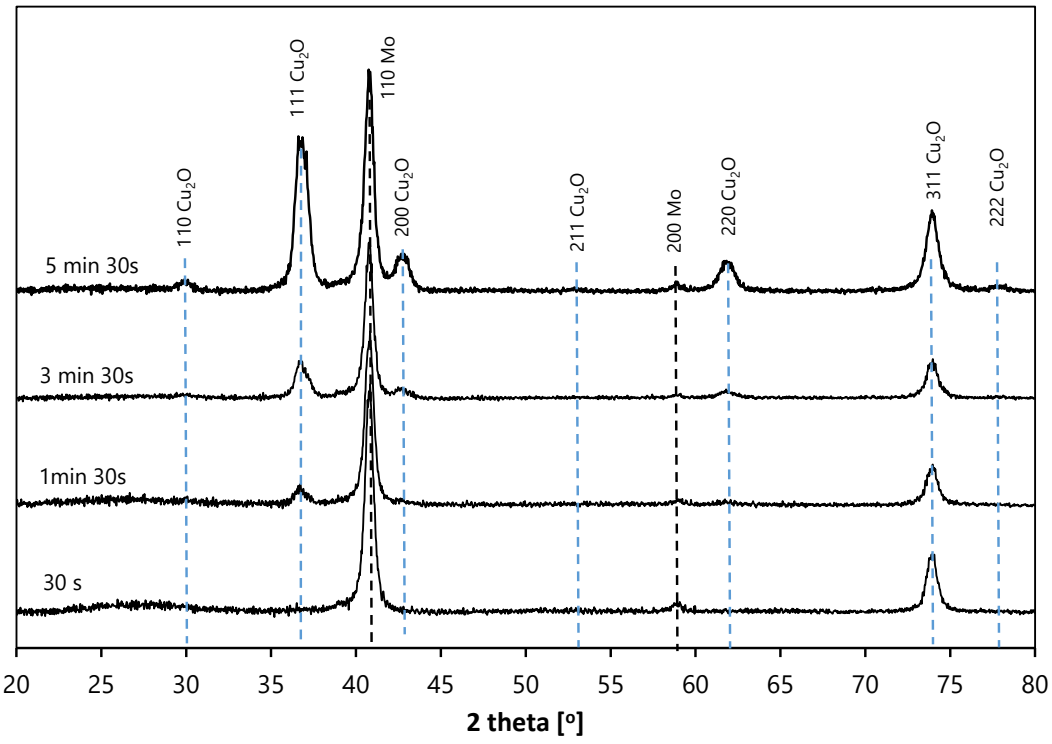

Figure 6. X-ray diffraction patterns of Cu_2O layer deposited at room temperature between 30 s and 5min30

Measurement of layer thickness by profilometer reveals that after 5 minutes of deposition, this seed layer reaches its maximum thickness, which is between 70 and 80 nm with or without glucose. Because the seed layer is continuous, it is possible to create a dense seeding array for heterogeneous nucleation. After 15 minutes, the particle size in the layer continues to increase (Figure 5 d,i). The thickness of the layers corresponds to the grain size. After 30 min of deposition, the shape of grains seems to become more defined. Indeed, based on our results, it appears that the growth of Cu_2O by CBD begins with germination (3D growth), then progresses to lateral growth, and finally to the stabilization of the deposit (2D growth). After one hour of deposition, no increase in the thickness of the layers is observed.

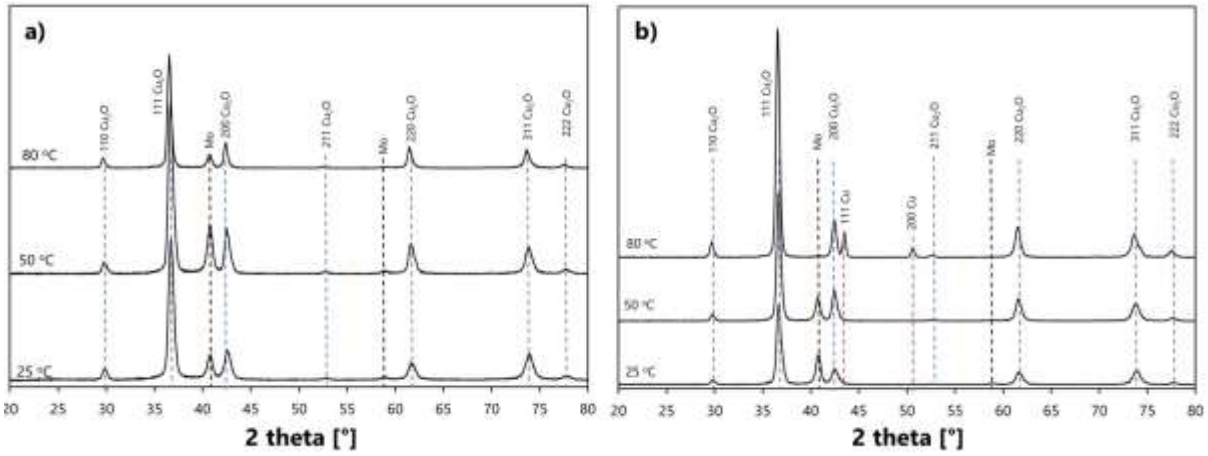

Figure 7. Thin film growth X-ray diffraction patterns as a function of temperature a) without and b) with glucose addition

3.4. The Influence of Reaction Temperature:

The effect of reaction temperature on the formation of Cu_2O layers was also studied at 25, 50, and 80°C for 1h of deposition at pH=10. Whatever the temperature, a pure Cu_2O layer forms. The intensity of the Mo peak decreases for a deposition temperature of 80°C compared to (111) Cu_2O reflection, indicating that the thickness of our layers is increasing. The preferred orientation of the crystals is (111). (Figure 7).

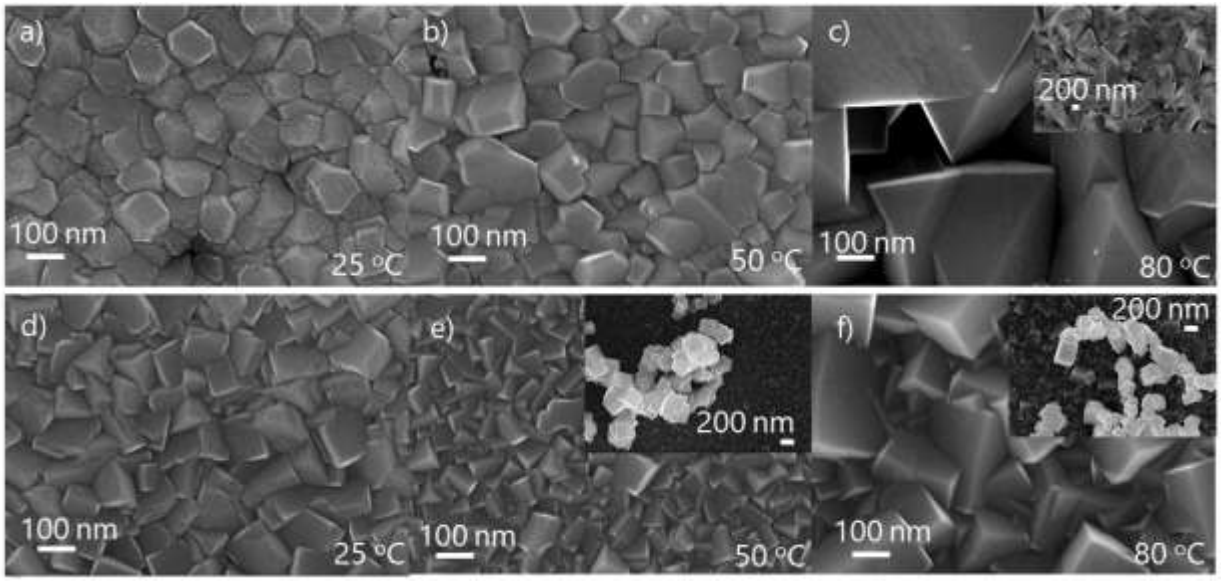

Figure 8: SEM images of Cu_2O deposition at 25°C, 50°C, and 80°C a,b,c) without glucose, d,e,f) with glucose for 1h

The surface of the layers is similar between 25 and 50°C but different at 80°C, according to SEM images (Figure 8). It is obvious that crystals formed at 80°C are significantly larger than those formed at 25 and 50 °C leading to thicknesses of around 400 nm. With the addition of glucose, we can see a relative homogeneity of the surface at 25 °C. At 50 and 80°C, however, some cubic crystals precipitate on the surface of the layers. At 80 °C, these cubes are more numerous and slightly larger. XRD analysis of the layers with the addition of glucose shows the presence of some peaks corresponding to pure Cu at 80 °C (Figure 6b). While the addition of glucose does not seem to have an impact on the composition of the layers at room temperature, increasing the temperature in the presence of a reducing agent seems to promote the formation of Cu^0.

The overall reaction for Cu_2O in the presence of a reducing agent can be written as:

$$2[CuT_2]^{2-} + RCHO + 5OH^- \rightarrow Cu_2O\ (s) + H_2\ (g) + 3H_2O + RCOO^- + 4T^{2-}$$

While the overall reaction leading to the formation Cu^0 reaction could be written as follows:

$$[CuT_2]^{2-} + 2RCHO + 4OH^- \rightarrow Cu^0\ (s) + H_2\ (g) + 2H_2O + 2HCOO^- + 2T^{2-}$$

At high temperatures these two reactions can come in competition, leading to co-precipitation of Cu_2O and Cu^0.

4. Discussion

The CBD technique is based on the gradual release of metal ions from a supersaturated solution for direct deposition of thin films. Typically, chelating agents are used to limit the hydrolysis of metal ions such as Cu and to add stability to a bath that would otherwise undergo rapid hydrolysis and precipitation. Our experiments revealed that the pH of the bath has a significant impact on supersaturation. At low pH, copper forms a strong complex with tartrate. As the pH rises, Cu reacts with OH^-, and copper-hydroxide complexes take over.

Copper-hydroxide complexes control supersaturation, which influences nucleation and growth rates. The degree of supersaturation is low at high pH, resulting in a low nucleation

rate and a relatively high growth rate, which results in a low nucleation site density and a large crystallite size. The density of nucleation sites increases while crystallite size decreases as pH decreases, which is consistent with the SEM results. Based on thermodynamic studies, it seems that well define and covering layers are growing mainly when copper-hydroxide and copper tartrate complexes co-existence in the solution. The amount of these complexes and their proportions depend on both the pH of the solution and the concentration of the tartrate with respect to the concentration of Cu ions ([tartrate]/[Cu]). The pH influences the concentration of Copper-hydroxide and copper tartrate complexes which in turn influences the nucleation rate, particle size, and morphology of the resulting Cu_2O thin films. This hypothesis has been confirmed experimentally, by adjusting the pH=10 and [tartrate]/[Cu]=10 leading to the formation of a homogeneous seed layer during the first few minutes of deposition. The increase in deposition time and the temperature mainly influence the grain size of copper oxides, which impacts the thickness of the layer. While the reducing agent (such as glucose) has not a real impact neither on the structure, nor on the growth of thin films layer at room temperature, at 80 °C, it favors the joint deposition of Cu_2O and metallic Cu. Thus the deposition of pure Cu_2O could be done easily at room temperature without the use of a reduction agent.

5. Conclusion

The growth mechanism of chemical bath deposition of Cu_2O thin film at room temperature has been analyzed based on thermodynamic studies. We showed that it is possible to deposit dense and homogenous cubic Cu_2O layers using a low-concentrated alkaline solution of copper (II) sulfate and sodium potassium tartrate $NaKC_4H_4O_6$ as a complexing agent by an appropriate and simultaneous adjustment of the solution's pH and [tartrate]/[Cu] concentration. A detailed thermodynamic study focuses on the effects of complexing agent concentration and pH on the solubility and speciation of copper hydroxo and copper tartrate complexes. It has been shown that increasing the pH accelerates the formation of Cu-hydroxo complexes, which controls supersaturation and has a direct impact on the nucleation and growth rates of thin films. Based on these studies we showed that dense and homogenous layers can only grow if both copper hydroxo and copper tartrate complexes are present in the solution.

The effect of pH variation and the addition of a reducing agent such as glucose on the structural properties and morphology of the films at room temperature revealed that pH has the greatest impact on crystal growth size and homogeneity, while the impact of the reducing agent such as glucose is negligible. The hydroxide anions appear to selectively stabilize the Cu_2O (111) facets regardless of pH, temperature, or reducing agent. However at higher temperatures (80 °C) the addition of glucose can lead to the co-precipitation of metallic Cu.

This work provides insights on the potential of analytical studies for a better understanding and optimization of chemical bath deposition of cuprous oxide films at room temperature which can find its application in various chemical and physical applications such as catalysts and absorbers for solar cells.

7. Appendix

Thermodynamic calculations

To carry out this theoretical study, a number of constants are required, including:

(1) $H^+ + OH^- = H_2O$ pKe = 14

For hydroxide species [38]

(2) $Cu^{2+} + OH^- = CuOH^+$ $\log \beta_1 = 6.5$

(3) $Cu^{2+} + 2OH^- = Cu(OH)_2$ $\log \beta_2 = 16.2$

(4) $Cu^{2+} + 3OH^- = [Cu(OH)_3]^-$ $\log \beta_3 = 26.6$

(5) $Cu^{2+} + 4OH^- = [Cu(OH)_4]^{2-}$ $\log \beta_4 = 39.7$

(6) $Cu^{2+} + 2OH^- = Cu(OH)_2$ $pK_s = 18.90$

For tartrate species

(7) $Cu^{2+} + T^{2-} = CuT$ $\log \beta_1 = 3.2$

(8) $Cu^{2+} + T_2^{4-} = [CuT_2]^{2-}$ $\log \beta_2 = 5.1$

(9) $Cu^{2+} + T_3^{6-} = [CuT_3]^{4-}$ $\log \beta_3 = 4.8$

(10) $Cu^{2+} + T_4^{8-} = [CuT_4]^{6-}$ $\log \beta_4 = 6.5$

(11) $H_2T = HT^- + H^+$ $pKa_1 = 3.22$

(12) $HT^- = T^{2-} + H^+$ $pKa_2 = 4.85$

For sulfate species

(13) $H_2SO_4 = HSO_4^- + H^+$ $pKa_1 = -1.91$

(14) $HSO_4^- = SO_4^{2-} + H^+$ $pKa_2 = 1.98$

(15) $Cu^{2+} + SO_4^{2-} = CuSO_4$ $\log K = 2.3$

References

[1] J. Ghijsen, L.H. Tjeng, J. van Elp, H. Eskes, J. Westerink, G.A. Sawatzky, M.T. Czyzyk, Electronic structure of Cu2O and CuO, Phys Rev B Condens Matter, 38 (1988) 11322-11330.

[2] C. Malerba, F. Biccari, C. Leonor Azanza Ricardo, M. D'Incau, P. Scardi, A. Mittiga, Absorption coefficient of bulk and thin film Cu2O, Solar Energy Materials and Solar Cells, 95 (2011) 2848-2854.

[3] B.K. Meyer, A. Polity, D. Reppin, M. Becker, P. Hering, P.J. Klar, T. Sander, C. Reindl, J. Benz, M. Eickhoff, C. Heiliger, M. Heinemann, J. Bläsing, A. Krost, S. Shokovets, C. Müller, C. Ronning, Binary copper oxide semiconductors: From materials towards devices, physica status solidi (b), 249 (2012) 1487-1509.

[4] S. Sun, Recent advances in hybrid Cu2O-based heterogeneous nanostructures, Nanoscale, 7 (2015) 10850-10882.

[5] S. Sun, X. Zhang, Q. Yang, S. Liang, X. Zhang, Z. Yang, Cuprous oxide (Cu2O) crystals with tailored architectures: A comprehensive review on synthesis, fundamental properties, functional modifications and applications, Progress in Materials Science, 96 (2018) 111-173.

[6] T. Minami, Y. Nishi, T. Miyata, J.-i. Nomoto, High-Efficiency Oxide Solar Cells with ZnO/Cu2O Heterojunction Fabricated on Thermally Oxidized Cu2O Sheets, Applied Physics Express, 4 (2011).

[7] T. Minami, Y. Nishi, T. Miyata, High-Efficiency Cu2O-Based Heterojunction Solar Cells Fabricated Using a Ga2O3Thin Film as N-Type Layer, Applied Physics Express, 6 (2013).

[8] T.K.S. Wong, S. Zhuk, S. Masudy-Panah, G.K. Dalapati, Current Status and Future Prospects of Copper Oxide Heterojunction Solar Cells, Materials (Basel), 9 (2016).

[9] X. Wan, J. Wang, L. Zhu, J. Tang, Gas sensing properties of Cu2O and its particle size and morphology-dependent gas-detection sensitivity, J. Mater. Chem. A, 2 (2014) 13641-13647.

[10] K.C. Christoforidis, P. Fornasiero, Photocatalysis for Hydrogen Production and CO2Reduction: The Case of Copper‐Catalysts, ChemCatChem, 11 (2018) 368-382.

[11] C. Qi, Y. Zheng, H. Lin, H. Su, X. Sun, L. Sun, CO oxidation over gold catalysts supported on CuO/Cu2O both in O2-rich and H2-rich streams: Necessity of copper oxide, Applied Catalysis B: Environmental, 253 (2019) 160-169.

[12] R.M. Aran-Ais, R. Rizo, P. Grosse, G. Algara-Siller, K. Dembele, M. Plodinec, T. Lunkenbein, S.W. Chee, B.R. Cuenya, Imaging electrochemically synthesized Cu2O cubes and their morphological evolution under conditions relevant to CO2 electroreduction, Nat Commun, 11 (2020) 3489.

[13] M. Schreier, J. Luo, P. Gao, T. Moehl, M.T. Mayer, M. Gratzel, Covalent Immobilization of a Molecular Catalyst on Cu2O Photocathodes for CO2 Reduction, J Am Chem Soc, 138 (2016) 1938-1946.
[14] I.V. Bagal, N.R. Chodankar, M.A. Hassan, A. Waseem, M.A. Johar, D.-H. Kim, S.-W. Ryu, Cu2O as an emerging photocathode for solar water splitting - A status review, International Journal of Hydrogen Energy, 44 (2019) 21351-21378.
[15] J. Luo, L. Steier, M.K. Son, M. Schreier, M.T. Mayer, M. Gratzel, Cu2O Nanowire Photocathodes for Efficient and Durable Solar Water Splitting, Nano Lett, 16 (2016) 1848-1857.
[16] A. Paracchino, V. Laporte, K. Sivula, M. Gratzel, E. Thimsen, Highly active oxide photocathode for photoelectrochemical water reduction, Nat Mater, 10 (2011) 456-461.
[17] C.Y. Toe, J. Scott, R. Amal, Y.H. Ng, Recent advances in suppressing the photocorrosion of cuprous oxide for photocatalytic and photoelectrochemical energy conversion, Journal of Photochemistry and Photobiology C: Photochemistry Reviews, 40 (2019) 191-211.
[18] M.B. Gawande, A. Goswami, F.X. Felpin, T. Asefa, X. Huang, R. Silva, X. Zou, R. Zboril, R.S. Varma, Cu and Cu-Based Nanoparticles: Synthesis and Applications in Catalysis, Chem Rev, 116 (2016) 3722-3811.
[19] S. Nandy, A. Banerjee, E. Fortunato, R. Martins, A Review on Cu_2O and Cu^{I}-Based p-Type Semiconducting Transparent Oxide Materials: Promising Candidates for New Generation Oxide Based Electronics, Reviews in Advanced Sciences and Engineering, 2 (2013) 273-304.
[20] A. Osherov, C. Zhu, M.J. Panzer, Role of Solution Chemistry in Determining the Morphology and Photoconductivity of Electrodeposited Cuprous Oxide Films, Chemistry of Materials, 25 (2013) 692-698.
[21] S. Haller, J. Jung, J. Rousset, D. Lincot, Effect of electrodeposition parameters and addition of chloride ions on the structural and optoelectronic properties of Cu2O, Electrochimica Acta, 82 (2012) 402-407.
[22] I.S. Brandt, M.A. Tumelero, S. Pelegrini, G. Zangari, A.A. Pasa, Electrodeposition of Cu2O: growth, properties, and applications, Journal of Solid State Electrochemistry, 21 (2017) 1999-2020.
[23] S. Yadav, A. Jain, P. Malhotra, A review on the sustainable routes for the synthesis and applications of cuprous oxide nanoparticles and their nanocomposites, Green Chemistry, 21 (2019) 937-955.
[24] M.D. Susman, Y. Feldman, A. Vaskevich, I. Rubinstein, Chemical deposition of Cu(2)O nanocrystals with precise morphology control, ACS Nano, 8 (2014) 162-174.
[25] T. Hildebrandt, N. Loones, M. Bouttemy, J. Vigneron, A. Etcheberry, D. Lincot, N. Naghavi, Toward a Better Understanding of the Use of Additives in Zn(S,O) Deposition Bath for High-Efficiency Cu(In,Ga)Se_2-Based Solar Cells, IEEE Journal of Photovoltaics, 5 (2015) 1821-1826.
[26] C. Hubert, N. Naghavi, B. Canava, A. Etcheberry, D. Lincot, Thermodynamic and experimental study of chemical bath deposition of Zn(S,O,OH) buffer layers in basic aqueous ammonia solutions. Cell results with electrodeposited $CuIn(S,Se)_2$ absorbers, Thin Solid Films, 515 (2007) 6032-6035.
[27] P. Fuchs, Y.E. Romanyuk, A.N. Tiwari, Chemical Bath Deposition, in: E.C. David Levy (Ed.) Transparent Conductive Materials, Wiley2018, pp. 81-103.
[28] S.M. Pawar, B.S. Pawar, J.H. Kim, O.-S. Joo, C.D. Lokhande, Recent status of chemical bath deposited metal chalcogenide and metal oxide thin films, Current Applied Physics, 11 (2011) 117-161.
[29] G. Hodes, Chemical Solution Deposition Of Semiconductor Films, Marcel Dekker, Inc., New York, 2002.
[30] H. Xu, J. Dong, C. Chen, One-step chemical bath deposition and photocatalytic activity of Cu2O thin films with orientation and size controlled by a chelating agent, Materials Chemistry and Physics, 143 (2014) 713-719.

[31] X. Zhao, Z. Bao, C. Sun, D. Xue, Polymorphology formation of Cu2O: A microscopic understanding of single crystal growth from both thermodynamic and kinetic models, Journal of Crystal Growth, 311 (2009) 711-715.
[32] M.D. Susman, Y. Feldman, A. Vaskevich, I. Rubinstein, Chemical Deposition and Stabilization of Plasmonic Copper Nanoparticle Films on Transparent Substrates, Chemistry of Materials, 24 (2012) 2501-2508.
[33] H. Xu, W. Wang, W. Zhu, Shape evolution and size-controllable synthesis of Cu2O octahedra and their morphology-dependent photocatalytic properties, J Phys Chem B, 110 (2006) 13829-13834.
[34] R. Zhang, X. Liu, T. Zhou, T. Zhang, Controllable construction of multishelled p-type cuprous oxide with enhanced formaldehyde sensing, J Colloid Interface Sci, 535 (2019) 58-65.
[35] B. Beverskog, I. Puigdomenech, Revised Pourbaix Diagrams for Copper at 25 to 300°C, Journal of The Electrochemical Society, 144 (1997) 3476-3483.
[36] A. Goux, T. Pauporté, J. Chivot, D. Lincot, Temperature effects on ZnO electrodeposition, Electrochimica Acta, 50 (2005) 2239-2248.
[37] S. Gallanti, E. Chassaing, D. Lincot, N. Naghavi, Influence of thiourea addition on the electrodeposition of ZnO from zinc nitrate aqueous solutions, Electrochimica Acta, 178 (2015) 225-233.
[38] K.J. Powell, P.L. Brown, R.H. Byrne, T. Gajda, G. Hefter, S. Sjöberg, H. Wanner, Chemical speciation of environmentally significant metals with inorganic ligands Part 2: The Cu2+-OH-, Cl-, CO32-, SO42-, and PO43- systems (IUPAC Technical Report), Pure and Applied Chemistry, 79 (2007) 895-950.
[39] Y.D. Gamburg, G. Zangari, Theory and Practice of Metal Electrodeposition, 2011.
[40] L. Wang, R. Zhang, T. Zhou, Z. Lou, J. Deng, T. Zhang, P-type octahedral Cu2O particles with exposed 111 facets and superior CO sensing properties, Sensors and Actuators B: Chemical, 239 (2017) 211-217.
[41] Q.-B. Ma, J.P. Hofmann, A. Litke, E.J.M. Hensen, Cu2O photoelectrodes for solar water splitting: Tuning photoelectrochemical performance by controlled faceting, Solar Energy Materials and Solar Cells, 141 (2015) 178-186.

Figure captions

Figure 6. Repartition of the copper species as a function of pH for 0.01 M, $CuSO_4$, and tartrate concentrations of a) 0 M b) 0.01M, [tartrate]/[Cu]=1, and c) 0.1 M, [tartrate]/[Cu]=5 and d) 0.25M, [tartrate]/[Cu]=10 at room temperature

Figure 7. The proportion of copper species as a function of tartrate concentration for pH of a) 7, b) 9, c) 10, and d) 12.

Figure 8: SEM images of Cu_2O layers deposited at pH between 9 and 12 without (left) and with (right) addition of glucose in the deposition bath

Figure 9. X-ray diffraction patterns of the Cu_2O layer deposited a) without and b) with glucose in the deposition bath at pH between 9 and 12

Figure 10. SEM images of Cu_2O layers deposited at pH 10 without (a-e) and with (f-j) addition of glucose at deposition times of (a,f) 30s, (b,g) 2min, (c,h) 4min, (d,i) 15 min and (e,j) 30 min

Figure 6. X-ray diffraction patterns of Cu_2O layer deposited at room temperature between 30 s and 5min30

Figure 7. Thin film growth X-ray diffraction patterns as a function of temperature a) without and b) with glucose addition

Figure 8: SEM images of Cu_2O deposition at 25 °C, 50 °C, and 80 °C a,b,c) without glucose, d,e,f) with glucose for 1h